Microscopic Analysis of the Valence Band and Impurity Band Theories of (Ga,Mn)As

J. Mašek,[1] F. Máca,[1] J. Kudrnovský,[1] O. Makarovsky,[2] L. Eaves,[2] R. P. Campion,[2] K. W. Edmonds,[2] A. W. Rushforth,[2] C. T. Foxon,[2] B. L. Gallagher,[2] V. Novák,[3] Jairo Sinova,[4,3] and T. Jungwirth[3,2]

[1]*Institute of Physics ASCR, v.v.i., Na Slovance 2, 182 21 Praha 8, Czech Republic*
[2]*School of Physics and Astronomy, University of Nottingham, Nottingham NG7 2RD, United Kingdom*
[3]*Institute of Physics ASCR, v.v.i., Cukrovarnická 10, 162 53 Praha 6, Czech Republic*
[4]*Department of Physics, Texas A&M University, College Station, Texas 77843-4242, USA*

(Received 28 July 2010; published 23 November 2010)

We analyze microscopically the valence and impurity band models of ferromagnetic (Ga,Mn)As. We find that the tight-binding Anderson approach with conventional parametrization and the full potential local-density approximation + U calculations give a very similar band structure whose microscopic spectral character is consistent with the physical premise of the $\boldsymbol{k}\cdot\boldsymbol{p}$ kinetic-exchange model. On the other hand, the various models with a band structure comprising an impurity band detached from the valence band assume mutually incompatible microscopic spectral character. By adapting the tight-binding Anderson calculations individually to each of the impurity band pictures in the single Mn impurity limit and then by exploring the entire doping range, we find that a detached impurity band does not persist in any of these models in ferromagnetic (Ga,Mn)As.

DOI: 10.1103/PhysRevLett.105.227202 PACS numbers: 75.50.Pp, 75.10.Lp, 75.30.Hx

Over more than four decades, (Ga,Mn)As has evolved from a pioneering direct gap p-doped semiconductor [1] into an archetypical degenerate semiconductor with hole-mediated ferromagnetism [2–4]. Paramagnetic insulating $Ga_{1-x}Mn_xAs$ materials prepared in the 1970s by melt growth showed valence band (VB) to impurity band (IB) activation, with a nonsystematic filamentary metallic conduction being observed at the highest studied dopings of $x \sim 0.1\%$ and ascribed to sample inhomogeneities [5]. The degenerate semiconductor regime was not reached in these materials. A comprehensive experimental assessment of basic doping only trends became possible in the late 1990s with the development of epitaxial (Ga,Mn)As films [2,6–8] which can be doped well beyond the equilibrium Mn solubility limit while avoiding phase segregation and maintaining a high degree of uniformity. Transport measurements on such films confirmed the insulating characteristics and the presence of the IB for $x \lesssim 0.1\%$. For higher concentrations, $0.5\% \lesssim x \lesssim 1.5\%$, no clear signatures of activation from the VB to the IB have been detected in the dc transport, suggesting that the bands start to overlap and mix, yet the materials remain insulating. At $x \sim 1.5\%$, the low-temperature conductivity of the films increases abruptly by several orders of magnitude and the material becomes a bulk degenerate semiconductor. The onset of ferromagnetism occurs on the insulating side of the transition at $x \sim 1\%$ and the Curie temperature gradually increases with increasing doping, reaching ~190 K at the accessible substitutional Mn_{Ga} doping of $x \sim 8\%$.

One physical scenario for ferromagnetic (Ga,Mn)As, termed the VB picture, has an exchange-split band structure comprising the impurity band merged into the valence band. The states at the Fermi energy E_F retain the predominant orbital character of the host semiconductor and are moderately hybridized with the localized Mn d electrons. This description, quantified by a variety of theoretical methods, has been a fruitful basis for analyzing and predicting a whole range of thermodynamic, magnetic, transport, and optical properties of ferromagnetic (Ga,Mn)As [3,4]. Recently, several experimental observations have been interpreted using alternative models of an IB which is detached from the VB [9–13]. However, it has been argued that a detailed analysis of the data in combination with transport experiments is also consistent with the VB picture [6]. The postulated IB models have not been previously derived from a microscopic theory considering all relevant orbital states in the mixed crystal. In order to help resolve the debate on these alternative interpretations, we examine here the IB models by recreating them using microscopic modeling techniques and studying their band-structure characteristics over the entire doping range. These calculations (i) firmly establish the microscopic basis and internal consistency of the VB picture, (ii) demonstrate the mutual inconsistency of the various postulated IB models, and (iii) demonstrate that a detached IB does not persist in any of the models' band structures at dopings corresponding to ferromagnetic (Ga,Mn)As. Our theoretical analysis is based on the tight-binding Anderson (TBA) approach which includes all spectral components in the band structure forming the states near E_F, accounts for the Mn d-orbital electron-electron interaction effects using the self-consistent unrestricted Hartree-Fock method, and can be adopted to realize microscopically the diverse proposed IB models. Additional physical insight is provided by comparisons to full-potential local-density approximation (LDA) and LDA + U calculations. More details on the

techniques and more extensive numerical results can be found in the supplementary material [14].

The perturbation of the crystal potential of GaAs due to a single Mn impurity has three components. (i) The first is the long-range hydrogeniclike potential of a single acceptor in GaAs which produces a bound state at about 30 meV above the VB [15]. (ii) The second contribution is a short-range central-cell potential. It is specific to a given impurity and reflects the difference in the electronegativity of the impurity and the host atom [16]. For a conventional nonmagnetic acceptor Zn_{Ga}, which is the 1st nearest neighbor of Ga in the periodic table, the atomic p levels are shifted by $\sim$0.25 eV, which increases the binding energy by $\sim$5 meV. For Mn, the 6th nearest neighbor of Ga, the p-level shift is $\sim$1.5 eV, which when compared to Zn_{Ga} implies the central-cell contribution to the acceptor level of Mn_{Ga} $\sim$30 meV [17]. (iii) The remaining part of the Mn_{Ga} binding energy is due to the spin-dependent hybridization of Mn d states with neighboring As p states. Its contribution, which has been directly inferred from spectroscopic measurements of uncoupled Mn_{Ga} impurities [17,18], is again comparable to the binding energy of the hydrogenic single-acceptor potential. Combining (i)–(iii) accounts for the experimental binding energy of the Mn_{Ga} acceptor of 0.1 eV. An important caveat to these elementary considerations, further quantified by our microscopic calculations [14], is that the short-range potentials alone of strengths inferred in (ii) and (iii) would not produce a bound state above the top of the VB but only a broad region of scattering states inside the VB.

The VB picture of ferromagnetic (Ga,Mn)As builds on the above conventional semiconductor description of the Mn_{Ga} acceptor in which the presence of the long-range hydrogeniclike impurity potential is essential for creating a bound state in the band gap. With increasing doping, the impurity level broadens, and for a sufficiently screened hydrogenic potential the impurity states must merge into the VB within this picture. The premise of the models with a persistent detached IB in ferromagnetic (Ga,Mn)As is distinct and can be reconciled by ascribing the main role in binding to the short-range potentials and a minor role to screening and impurity level broadening.

We now provide microscopic analysis of these scenarios by performing TBA band-structure calculations. Disorder is treated in the coherent potential approximation (CPA) which allows us to scan the entire range of dopings from the single Mn-impurity limit to MnAs. Our results are consistent with available corresponding spectra obtained using the supercell method [19] which justifies the validity of the CPA [14] to represent the one-particle, orbital resolved, density of states (DOS). We first take the conventional parametrization of atomic levels and overlap integrals [14,16]. On-site electron-electron interactions on the Mn d states are described using the Hubbard parameter $U = 3.5$ eV and the Heisenberg parameter $J_H = 0.6$ eV, which also correspond to a conventional parametrization of d-orbital correlations in atomic Mn or Mn in II-VI semiconductors, and are consistent with values of U and J_H inferred from photoemission experiments in (Ga,Mn)As [20]. Since we are primarily interested in the ferromagnetic behavior which occurs at relatively high dopings ($\gtrsim$1%) and is governed by the spin-dependent p-d hybridization potential, we omit the long-range Coulomb potential which is nonmagnetic and largely screened at the relevant hole concentrations [21].

Using the conventional values of the TBA parameters [14,16], we first determined occupation numbers on Mn d orbitals and corresponding on-site energies using the self-consistent unrestricted Hartree-Fock description of the Anderson Mn impurity embedded in the semiconductor environment [14]. The important result of these calculations is that we did not find any tendency to symmetry breaking in these occupation numbers; i.e., the three t_{2g} orbitals (and similarly the two weakly hybridized e_g orbitals) remain degenerate and strongly localized. After determining the Mn d orbital on-site energies we proceed to calculate the microscopic DOS of (Ga,Mn)As over the entire doping range. In Figs. 1(a) and 1(b) we plot examples of both the total (black line) and the Mn d-orbital resolved [gray (red) filled areas] DOSs for $x = 3\%$, 6%, and 12% together with the results for $x = 100\%$, i.e., for the zinc-blende MnAs. The Mn d spectral weight is peaked at approximately 4 eV below the top of the VB, in agreement with photoemission data [20], and is significantly smaller near E_F as further highlighted in Fig. 2(b). The Fermi level states at the top of the VB have a dominant As(Ga) p-orbital character; the stronger As p component is plotted in Figs. 2(a). The p-d coupling strength,

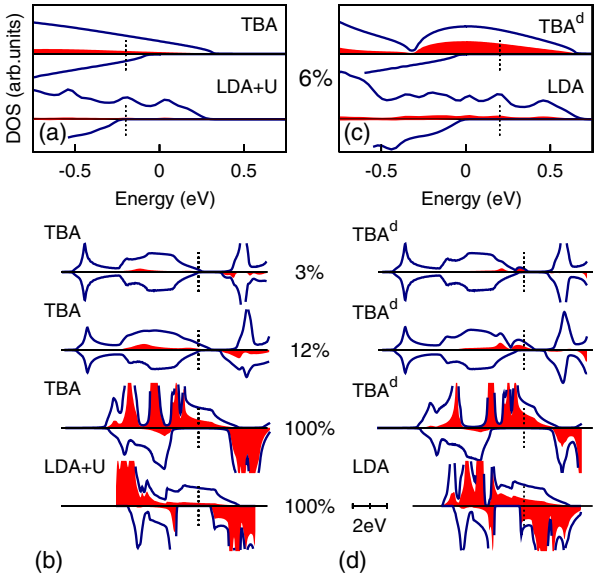

FIG. 1 (color online). (a),(b) Total (solid line) and partial Mn d-orbital [gray (red) filled areas] DOSs calculated using the TBA (CPA) and compared with the LDA + U (supercell) results for Mn_{Ga} dopings of 3%, 6%, 12%, and 100%. (c),(d) Same for the TBA^d compared with the LDA results. E_F is indicated by the dashed vertical line.

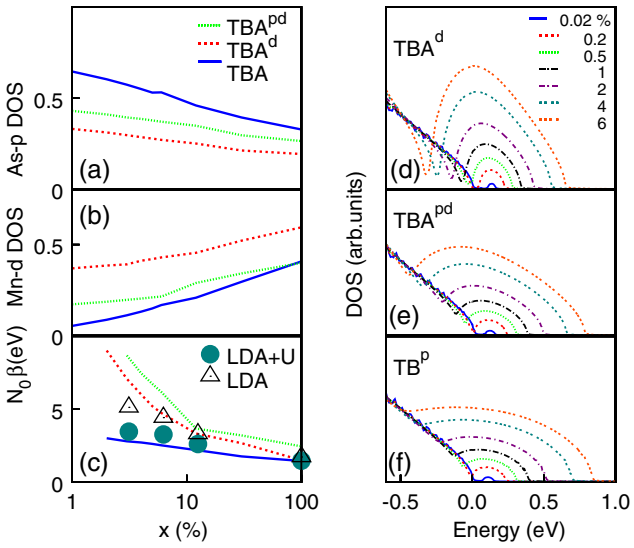

FIG. 2 (color online). Partial As p-orbital (a) and Mn d-orbital (b) DOSs at E_F in the depicted TBA models. The remaining contribution to the total DOS is primarily due to Ga and Mn p orbitals with their relative weights given nearly precisely by the Ga/Mn ratio [14]. (c) The p-d coupling strength in the TBA models compared with the LDA (triangles) and LDA + U (circles) results. (d)–(f) Total DOSs showing the merging of the IB into the VB in the depicted tight-binding models.

$N_0\beta = \Delta/(Sx)$ [3], determined from the calculated VB exchange splitting Δ (and taking $S = 5/2$), is close to the upper bound of the reported experimental range of $N_0\beta \sim 1$–3 eV [17,20,22–24], as shown in Fig. 2(c). This is regarded as a moderately weak p-d coupling because the corresponding Fermi level states of the (Ga,Mn)As have a similar orbital character as the states in the host GaAs VB. The spectral features shown in Figs. 1(a), 1(b), and 2(a)–2(c) are among the key characteristics of the VB picture. Note that the $\boldsymbol{k}\cdot\boldsymbol{p}$ kinetic-exchange (Zener) model calculations assume a value of $N_0\beta$ also within the range of 1–3 eV (typically closer to the lower experimental bound) [3]. It is this moderate p-d hybridization that allows it to be treated perturbatively and to perform the Schrieffer-Wolff transformation to effective valence band states experiencing a spin-dependent kinetic-exchange field [3]. Hence, the effective kinetic-exchange model and the microscopic TBA theory provide a consistent physical picture of ferromagnetic (Ga,Mn)As.

We next attempt to recreate the IB models by considering that the bound state at the single Mn is formed by the short-range impurity potentials. As noted above, this is not obtained from the conventionally parametrized TBA, and the values of the atomic levels or overlap integrals have to be adjusted *ad hoc* to match the 0.1 eV binding energy [14]. We first search for a bound state due to the central-cell potential by treating the Mn p level as a free parameter. We find that binding the hole by the central-cell potential alone requires physically incomprehensible p-level shifts of several tens of eV [25]. The reason for this is the short-range nature of the potential and the orbital composition of the top VB from which the bound state forms. The VB near its maximum is dominated by p orbitals of the As not Ga sublattice.

A more favorable scenario to create a bound state through the short-range potentials is tuning the strength of the p-d hybridization. This term is less local as it affects four As neighbors of the Mn_{Ga} impurity and acts on the As p orbitals which form the top of the host VB. To tune the hybridization strength we can treat as a free parameter the atomic Mn d level or the p-d hopping [14]. The corresponding models are labeled as TBA^d and TBA^{pd}, respectively. For the TBA^d model we obtain the 0.1 eV bound state when shifting the d level by 1.5 eV. We now fix this parameter and calculate the corresponding DOSs over the entire doping range, as shown in Figs. 1(c) and 1(d). More detailed characteristics of the corresponding spectra are summarized in Figs. 2(a)–2(d). The key observation is that for dopings above $\sim$0.1% the band structure cannot be recast in a model with Fermi level states residing in a narrow IB (of width not exceeding the single impurity binding energy) which is detached from the VB. The TBA^{pd} model yields the same general conclusion, as shown in Figs. 2(d) and 2(e). A detached IB model for the ferromagnetic (Ga,Mn)As materials is therefore microscopically incompatible with the 0.1 eV acceptor level even if the binding of the hole to the Mn impurity was entirely due to short-range potentials. We remark that $N_0\beta$ in the $TBA^{d(pd)}$ parametrization is about a factor of 2–3 stronger than in the conventionally parametrized TBA model, i.e., much larger than the upper experimental bound for the p-d coupling strength. This discrepancy is due to the omission of the long-range Coulomb potential when fitting the experimental single Mn_{Ga} acceptor state. Note also that the dip in the $TBA^{d(pd)}$ DOS, which persists and shifts deep in the band at high dopings, is another consequence of the *ad hoc* increased p-d coupling.

We next associate the IB models postulated in literature with corresponding microscopic TBA calculations. One proposed phenomenology assumes a dominant Mn d-orbital nature of the detached IB and allows for some hybridization with the host VB [9,13]. The TBA^d theory is the closest microscopic realization of this model. It shows that apart from the absence of the detached IB itself at dopings corresponding to ferromagnetic (Ga,Mn)As, the formation of the 0.1 eV acceptor state by shifting the Mn d level does not yield a dominant Mn d spectral weight near E_F. From this perspective we regard the 0.1 eV acceptor level as moderately shallow.

An orthogonal IB model, in terms of the assumed orbital character of the IB, elaborates on a sp-tight-binding Hamiltonian with shifted p levels on four As neighbors of the Mn_{Ga} [12]. We label this model as TB^p. The shifts are introduced to effectively account for the microscopic p-d hybridization and again to obtain the 0.1 eV single impurity state without the hydrogenic long-range Coulomb potential. The model has a merit in the very dilute regime [25] as the extent of the bound-state wave function (the

exponential tail) is determined by the value of the binding energy and is insensitive to the specific choice of the confining potential. It also captures, by its design, the symmetries of the As p-orbital dominated bound state. The model can be associated with our microscopic TBA^{pd} calculations, and indeed the corresponding DOSs show very similar doping trends, as shown in Figs. 2(e) and 2(f). Again, no detached IB persists in the TB^{p} DOS to dopings above $\sim 0.1\%$.

Another phenomenological proposal assumes that states in the IB have Mn p-orbital character [10]. This corresponds to our first attempt to obtain the $\mathrm{Mn_{Ga}}$ acceptor level in short-range potentials by considering the central-cell component only. As discussed above, such a model would require an unphysical large shift of the Mn p levels. If we omit the microscopic justification of this IB model the approach has merit as a phenomenological effective model describing the Mn acceptor level in the band gap of the host semiconductor. Since the impurity states are added in this type of effective modeling *ad hoc* to the spectrum, the model does not conserve the total number of states. (In a microscopic language it describes an interstitial rather than a substitutional impurity.) The applicability of the approach is therefore limited to small Mn concentrations, and the model is not suitable for exploring trends with changing Mn doping.

Finally we show in Figs. 1(a)–1(d) examples of the comparisons of the TBA^{d} and TBA calculations with results of the LDA and LDA + U full-potential *ab initio* theories [14,26]. We find a very good agreement between the TBA and LDA + U results [27]. The LDA + U, the TBA, and the kinetic-exchange Zener theories therefore all provide a compatible picture of the band structure of ferromagnetic (Ga,Mn)As. We also find a clear correspondence between the TBA^{d} and LDA results. The large exchange splitting of the VB obtained in the LDA reflects the general deficiency of the LDA to account for localized states within an itinerant band. Mn d states are more delocalized and move closer to the VB edge in the LDA, which enhances the hybridization. Hence, the exchange splitting of the top of the VB is increased to values comparable to those of the TBA^{d} Hamiltonian.

To conclude, at the doping levels for which (Ga,Mn)As is ferromagnetic none of the postulated one-particle DOS models with a detached IB arising from the 0.1 eV Mn acceptor level in GaAs is microscopically justified. The Fermi level states in ferromagnetic (Ga,Mn)As can be regarded as residing in a modified VB of the host semiconductor due to disorder, exchange splitting, and admixture of the impurity orbitals. The corresponding one-particle band structure can be described by methods ranging from full-potential density-functional theory to multiorbital tight-binding Anderson or envelope-function approaches which are all mutually consistent. We also emphasize, nevertheless, that due to the vicinity of the metal-insulator transition and correlation phenomena these effective one-particle VB band models can only represent a proxy to the complex electronic structure of ferromagnetic (Ga,Mn)As materials.

We acknowledge support from EU Grants FP7-215368 SemiSpinNet, FP7-214499 NAMASTE, Czech Republic Grants GACR 202/07/0456, AV0Z10100520, AV0Z10100521, KAN400100652, LC510, Preamium Academiae, and U.S. Grants ONR-N000140610122, DMR-0547875, SWAN-NRI, and NSF-MRSEC DMR-0820414. J. S. acknowledges financial support through a Cottrell Scholar Award from the Research Corporation.

[1] R. A. Chapman and W. G. Hutchinson, Phys. Rev. Lett. **18**, 443 (1967).
[2] H. Ohno, Science **281**, 951 (1998).
[3] T. Jungwirth *et al.*, Rev. Mod. Phys. **78**, 809 (2006).
[4] *Spintronics*, edited by T. Dietl *et al.*, Semiconductors and Semimetals Vol. 82 (Elsevier, New York, 2008).
[5] D. A. Woodbury and J. S. Blakemore, Phys. Rev. B **8**, 3803 (1973).
[6] T. Jungwirth *et al.*, Phys. Rev. B **76**, 125206 (2007).
[7] V. Novák *et al.*, Phys. Rev. Lett. **101**, 077201 (2008).
[8] M. Wang *et al.*, Appl. Phys. Lett. **93**, 132103 (2008).
[9] K. S. Burch *et al.*, Phys. Rev. Lett. **97**, 087208 (2006).
[10] P. R. Stone *et al.*, Phys. Rev. Lett. **101**, 087203 (2008).
[11] K. Ando *et al.*, Phys. Rev. Lett. **100**, 067204 (2008).
[12] J.-M. Tang and M. E. Flatté, Phys. Rev. Lett. **101**, 157203 (2008).
[13] K. S. Burch, D. D. Awschalom, and D. N. Basov, J. Magn. Magn. Mater. **320**, 3207 (2008).
[14] See supplementary material at http://link.aps.org/supplemental/10.1103/PhysRevLett.105.227202 for details on the theory formalism and additional theoretical results.
[15] M. P. Marder, *Condensed Matter Physics* (Wiley, New York, 2000); see also the supplementary material [14].
[16] W. A. Harrison, *Electronic Structure and the Properties of Solids* (Freeman, San Francisco, 1980).
[17] A. K. Bhattacharjee and C. B. à la Guillaume, Solid State Commun. **113**, 17 (1999).
[18] M. Linnarsson *et al.*, Phys. Rev. B **55**, 6938 (1997).
[19] M. Turek, J. Siewert, and J. Fabian, Phys. Rev. B **78**, 085211 (2008).
[20] J. Okabayashi *et al.*, Phys. Rev. B **58**, R4211 (1998).
[21] From the technical viewpoint, the tight-binding approach is not well suited to account for long-range potentials.
[22] F. Matsukura *et al.*, Phys. Rev. B **57**, R2037 (1998).
[23] J. Szczytko *et al.*, Phys. Rev. B **59**, 12 935 (1999).
[24] T. Omiya *et al.*, Physica (Amsterdam) **7E**, 976 (2000).
[25] J.-M. Tang and M. E. Flatté, Phys. Rev. Lett. **92**, 047201 (2004).
[26] A. B. Shick, J. Kudrnovský, and V. Drchal, Phys. Rev. B **69**, 125207 (2004); L. M. Sandratskii, P. Bruno, and J. Kudrnovský, *ibid.* **69**, 195203 (2004); M. Wierzbowska, D. Sanchez-Portal, and S. Sanvito, *ibid.* **70**, 235209 (2004).
[27] Note that the only marked difference between the TBA and LDA + U results is in the semiconductor band gap underestimated in the density-functional theories.